Volume 51
Number 13
7 April 2022
Pages 4931-5338

Dalton Transactions

An international journal of inorganic chemistry

rsc.li/dalton

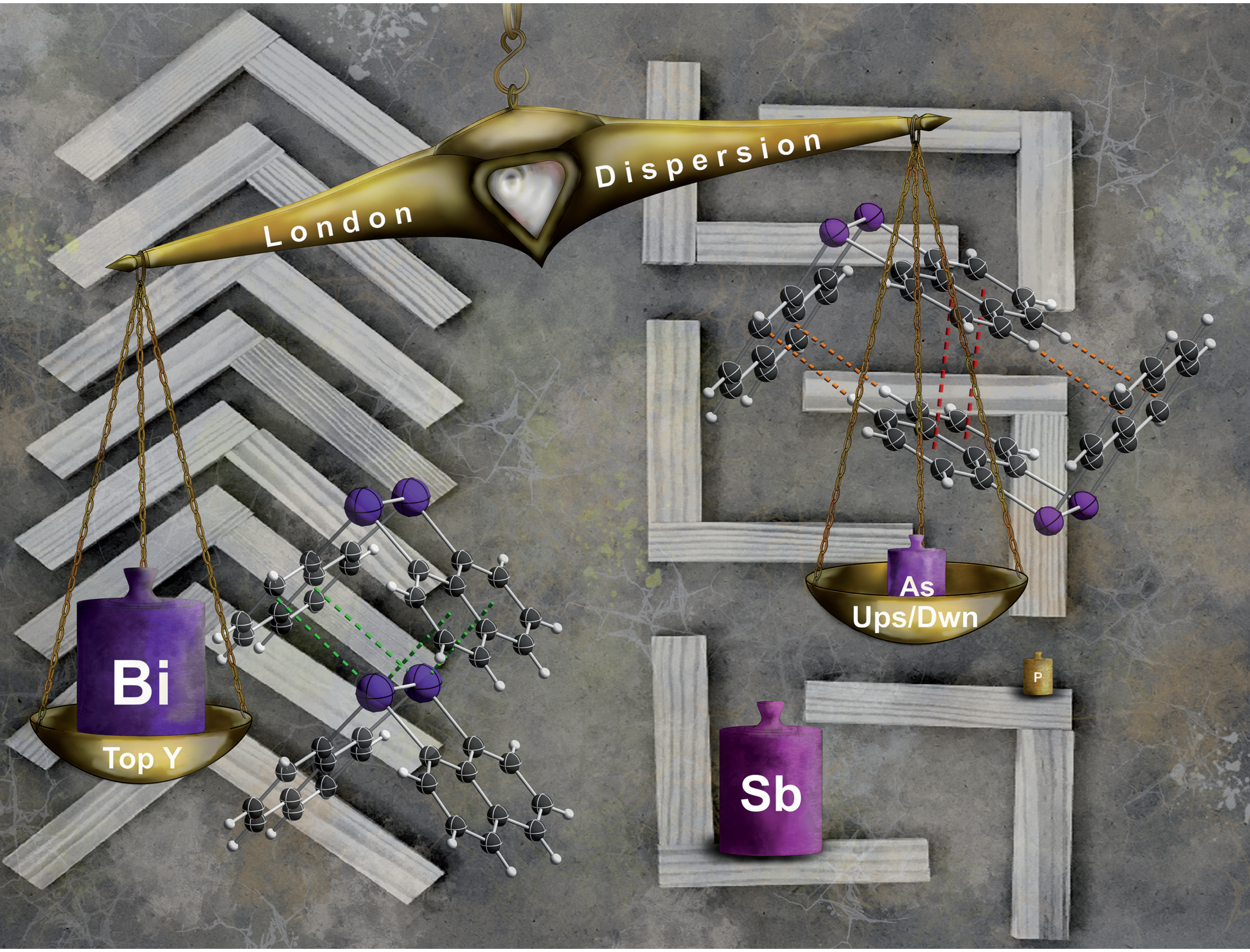

ISSN 1477-9226

ROYAL SOCIETY OF CHEMISTRY

PAPER
Alexander A. Auer, Stephan Schulz *et al.*
Comparing London dispersion pnictogen–π interactions in naphthyl-substituted dipnictanes

Dalton Transactions

ROYAL SOCIETY OF CHEMISTRY

PAPER

View Article Online
View Journal | View Issue

Open Access Article. Published on 01 March 2022. Downloaded on 2/14/2026 10:43:23 PM. This article is licensed under a Creative Commons Attribution-NonCommercial 3.0 Unported Licence.

Check for updates

Cite this: *Dalton Trans.*, 2022, **51**, 5016

Received 15th February 2022,
Accepted 1st March 2022

DOI: 10.1039/d2dt00477a

rsc.li/dalton

Comparing London dispersion pnictogen–π interactions in naphthyl-substituted dipnictanes†

Alexander Gehlhaar,[a] Eduardo Schiavo,[b] Christoph Wölper,[a] Yannick Schulte,[a] Alexander A. Auer*[b] and Stephan Schulz *[a,c]

Using a combination of NMR, single crystal X-ray diffraction (sc-XRD) and quantum chemistry, the structure-directing role of London Dispersion (LD) is demonstrated for dibismuthane Bi_2Naph_2 (**1**). **1** shows intermolecular Bi⋯π contacts in the solid-state, while π⋯π interactions as observed in the lighter homologues are missing. Comparison of the whole series of dipnictanes revealed the influence of the pnictogen atom on the strength of London dispersion and highlights its importance in heavy main group element chemistry.

Introduction

In the last decade, the structure directing role of London dispersion forces (LDF) has been intensively studied.[1,2] LDF were found to significantly contribute to the energetic stabilization of a variety of compounds by overcompensating repulsive interactions between the ligands resulting from Pauli interaction of the electron clouds.[3] Apart from LD interactions between organic ligands, easy polarizable metal atoms such as heavy p-block metals are also suitable to form attractive metal–metal[4] and metal–ligand interactions.[5] *Peri*-substituted naphthalene (naph) metal complexes are promising candidates to investigate LD interactions due to the structural rigidity of the planar naphthalene skeleton and the proximity of the groups in 1,8-position.[6] While this was shown for pnictogen-substituted (**I**, **II**, (Fig. 1))[7–9] and heteroatomic Au⋯Sb and Hg⋯Sb naphthalene complexes,[10] *peri*-substituted species containing the heaviest and easily polarizable group 15 elements, Sb and Bi,[11] are still rare. Dipnictanes Pn_2Naph_2 (Pn = As, Sb; type **V**) were structurally characterized,[12] with Sb_2Naph_2 forming dimers in the solid-state resulting from dispersion-dominated Sb⋯π interactions, whereas the corresponding diarsane and diphosphane Pn_2Naph_2 (Pn = P,[13] As[12b]) lack any Pn based LD interactions, most likely due to the poorer polarizability of As compared to Sb. In addition, Bi⋯π interactions were recently observed in $Ph_2Bi_2Naph_2$ (type **IV**).[9] To compare the role of LDF in dipnictanes Pn_2Naph_2, we became interested in the structure of the missing member, Bi_2Naph_2, since Bi as the largest and softest group 15 element according to the HSAB (hard–soft-acid–base) principle is an ideal candidate for the formation of noncovalent inter- and intramolecular interactions.

Results and discussion

Bi_2Naph_2 (**1**) was prepared by slow addition of $BiCl_3$ to a cooled solution (−30 °C) of Li_2Naph in thf and colorless crystals of **1** were isolated after workup and characterized by NMR and IR spectroscopy, elemental analysis and sc-XRD (Scheme 1).

The ^1H NMR of **1** in thf-d_8 shows the typical doublet of doublets (8.11 ppm, 7.35 ppm, 7.31 ppm), that were also observed for the lighter homologues.

1 crystallizes in the monoclinic space group $C2/c$ with eight molecules per unit cell (Fig. 2A). The Bi–Bi bond length in **1**

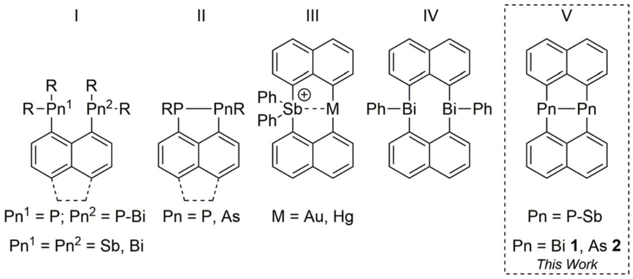

Fig. 1 *Peri*-substituted group 15 naphthalene/acenaphthene complexes.

---

[a] *Institute for Inorganic Chemistry, University of Duisburg-Essen, Universitätsstraße 5-7, D-45117 Essen, Germany. E-mail: stephan.schulz@uni-due.de*

[b] *Max-Planck-Institut für Kohlenforschung, D-45470 Mülheim an der Ruhr, Germany. E-mail: alexander.auer@kofo.mpg.de*

[c] *Center for Nanointegration Duisburg-Essen (Cenide), University of Duisburg-Essen, Germany*

† Electronic supplementary information (ESI) available: Experimental, analytical (NMR and IR spectra, elemental analysis) and computational details of **1** and **2**. CCDC 2125603 (**1**) and 2125604 (**2**). For ESI and crystallographic data in CIF or other electronic format see DOI: 10.1039/d2dt00477a

This journal is © The Royal Society of Chemistry 2022

Open Access Article. Published on 01 March 2022. Downloaded on 2/14/2026 10:43:23 PM.
This article is licensed under a Creative Commons Attribution-NonCommercial 3.0 Unported Licence.

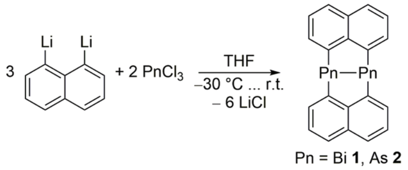

Scheme 1 Synthesis of **1** and **2**.

(2.8964(8) Å) is at the shorter end of Bi–Bi single bond lengths and the avg. sum of bond angles (261.25°) is smaller than those of the lighter Pn_2Naph_2 homologues (Pn = Sb 267.23°, As 278.11°, P 286.11°), clearly reflecting the increasing p-orbital character in the bonding electron pairs and the increasing s-character of the Pn electron lone pairs with increasing atomic number. More importantly, the molecular packing of **1** significantly deviates from their lighter homologues Pn_2Naph_2.[12,13] **1** does not show any π⋯π contacts as was observed in the lighter homologues, but two Bi⋯π contacts per Bi atom were observed (Fig. 2D). In contrast, only one Sb⋯π contact was found in Sb_2Naph_2 and even none in the lightest homologues (P, As), respectively. Moreover, the Bi⋯π distances in **1** (3.69 Å/3.58 Å, 3.81 Å/3.80 Å) are almost identical to the Sb⋯π distances in Sb_2Naph_2 (3.65 Å, 3.86 Å) despite the larger atomic radius of Bi, indicating stronger intermolecular interactions. Furthermore, Bi⋯H contacts were observed (Fig. 2B), forming a zig-zag chain through the interaction of two hydrogens with a Bi atom (Fig. 2C), which are further connected *via* H⋯H and CH⋯π contacts (Fig. 2D).

The same synthetic procedure was also applied for the diarsane and distibane complexes. Recrystallising a sample of As_2Naph_2 (**2**) from fluorobenzene yielded a new polymorph in the triclinic space group $P\bar{1}$.

The bonding parameters of diarsane **2** are in close proximity to those of the first polymorph (CCDC-1907994, ref. code HOJVAG).[12] However, **2** shows intermolecular As⋯As contacts in contrast to the initially reported structure, which are accompanied by π⋯π and CH⋯π contacts (Fig. 3).

To understand why **1** and **2** form different intermolecular interactions in the crystal, a computational analysis of both structures was carried out. Using a cluster approach that has proven to yield robust and accurate results,[13,14] we computed and analysed all relevant intermolecular interactions and the approximated cohesion energies in the different structures. The findings show that the stability of a crystal structure can be rationalized in terms of dimer interactions, and a comparison of interaction energies for possible dimers of Pn_2Naph_2 (Pn = P–Bi) yields an explanation why only Bi shows a structure with the unique stacking motif.

Before turning to the crystal structure models, the two most relevant dimers in **1** are used to benchmark our methodology as outlined in the following: the dimer structures (Fig. 4) from

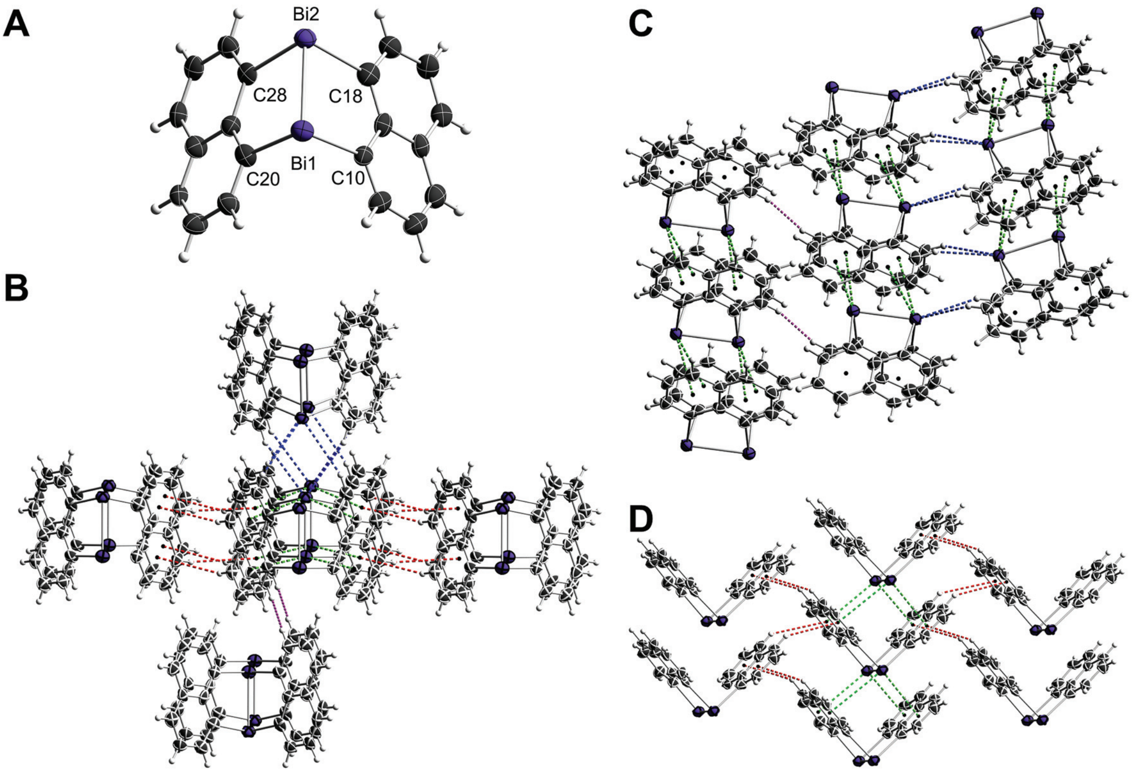

Fig. 2 (A) The solid-state structure of **1** with displacement ellipsoids drawn at the 50% probability level. Selected bond lengths (Å) and angles (°), **1**: Bi1–Bi2 2.8964(8), Bi1–C10 2.241(13), Bi1–C20 2.271(15), Bi2–C18 2.264(16), Bi2–C28 2.249(14), C10–Bi1–C20 89.1(5), C10–Bi1–Bi2 85.2(3), C20–Bi1–Bi2 84.7(3), C18–Bi2–C28 92.2(5), C18–Bi2–Bi1 85.4(4), C28–Bi2–Bi1 85.9(3). (B–D) Crystal packing of **1**. One Bi_2Naph_2 molecule is connected with nine surrounding Bi_2Naph_2 molecules through H⋯H (pink), CH⋯π (orange), Bi⋯H (blue) and Bi⋯π (green) contacts.

Open Access Article. Published on 01 March 2022. Downloaded on 2/14/2026 10:43:23 PM.
This article is licensed under a Creative Commons Attribution-NonCommercial 3.0 Unported Licence.

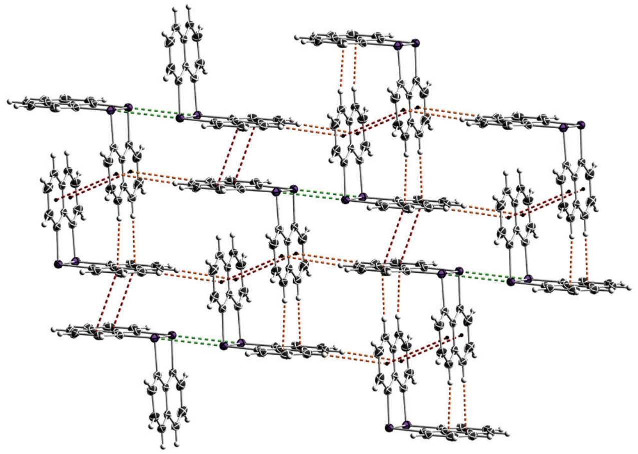

Fig. 3 Crystal packing of **2**. The As_2Naph_2 molecules form a two-dimensional network, which is connected *via* π⋯π (red), CH⋯π (orange) and As⋯As (green) contacts.

sc-XRD were kept frozen and the energies of the dimer and monomers were computed at the DLPNO-CCSD(T)/cc-pVTZ level of theory[12,15–19] and with the B3LYP,[20] PBE,[21] PBE0,[22] TPSS,[23] M06-2x[24] and BP86[25] functionals (def2-TZVPP basis set[26] and D3-BJ correction[27,28]). The Local Energy Decomposition (LED) was used to extract the dispersion component from the DLPNO-CCSD(T) calculations.[29,30] Calculations were run with ORCA (version 5.0),[31] and all further analyses were carried out with PBE0.

Compared to the other widely used functionals (*e.g.* TPSS and PBE), which in their corrected versions accurately describe interaction energies and their components in agreement with previous studies,[30,32–34] PBE0 has shown a reasonable accuracy on both, dispersive and non-dispersive (electrostatic, charge-transfer and covalent) contributions (for more details, see ESI†).

Having established that DFT results offer an excellent balance between cost and accuracy, a cluster approach to compute interaction energies was applied to the crystal structure of **1**. The central molecule surrounded by its nearest neighbours was chosen as model system. From a 13-molecule cluster, all possible dimers containing the central molecule and its nearest neighbours were isolated (Fig. 5). The top of Fig. 5A shows the dimers that are most relevant to the total structure (*vide infra*), while at the bottom less important dimers are displayed.

Fig. 5B shows a comparison of the interaction energies of the different dimers from the molecular structures fixed at the crystallographic geometries. The comparison reveals that some dimers contribute to a larger extent to the stability of the crystal structure than others. It must be noted that the different contributions need to be weighted based on how many times a particular dimer motif occurs in the cluster.

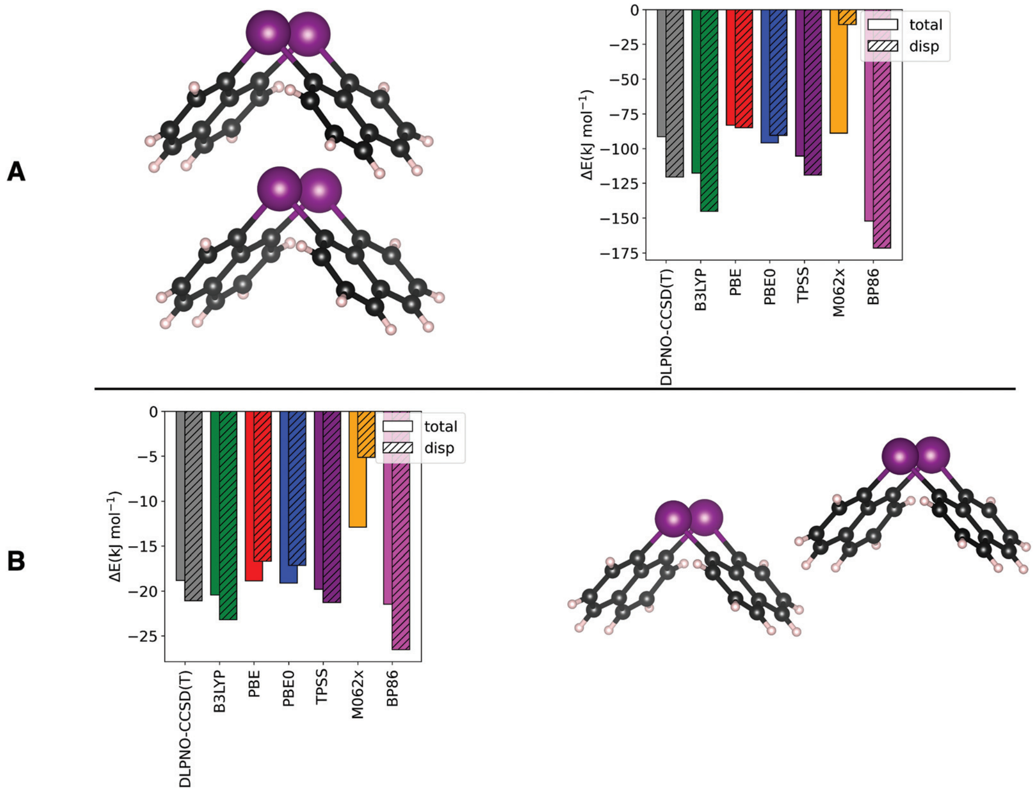

Fig. 4 Benchmark of DFT-D3 functionals against DLPNO-CCSD(T) on the dimer formation energy of Top Y (A) and Side X (B). See Fig. 2 for the dimers naming convention. DLPNO-CCSD(T) calculations were run with the cc-pVTZ basis set and DFT-D3 with the def2-TZVPP basis.

Open Access Article. Published on 01 March 2022. Downloaded on 2/14/2026 10:43:23 PM.
This article is licensed under a Creative Commons Attribution-NonCommercial 3.0 Unported Licence.

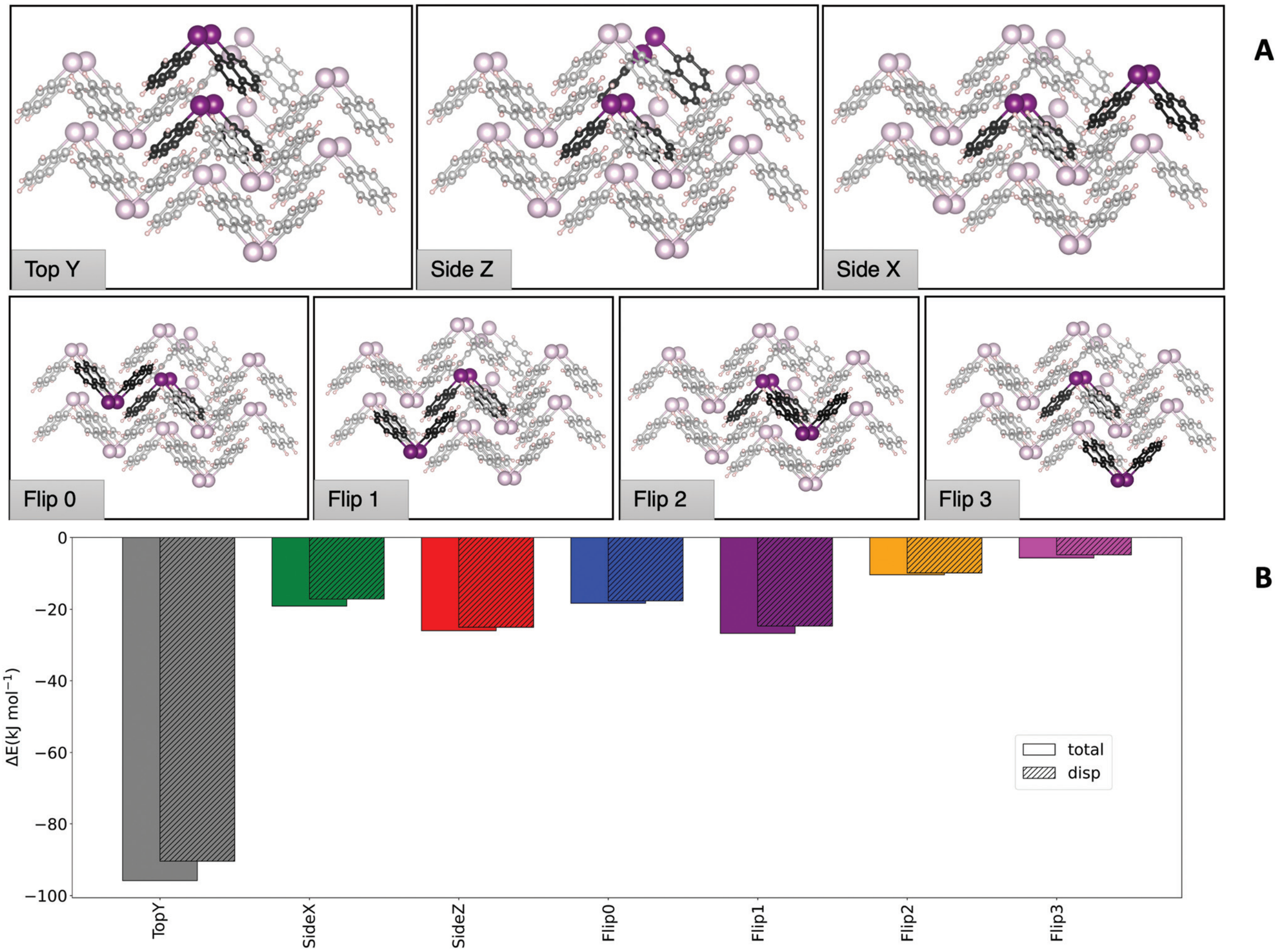

Fig. 5 (A) Dimers as cut from the 13-molecule cluster of Bi_2Naph_2 (**1**). Geometries are frozen at the experimental crystallographic ones. The highlighted molecules are the ones included in the calculations (see text) while the rest of the cluster is only shown to illustrate how the dimers were extracted. Colour code: C (black), Bi (purple), H (light pink). (B) Comparison between the different dimer formation energies at the PBE0/def2-TZVPP level of theory.

Symmetry considerations show that the 'Top Y' and 'Side Z' interactions are found twice in the cluster, while the 'Side X' interaction appears four times and all others only once. Hence, these three motifs play a major role in the formation of this structure, with 'Top Y' being by far the most important one. Consistently with what has been observed before in similar studies,[12] LDF accounts for a large part of the total interaction for all dimers.

The approximated cohesion energy, defined as the energy to insert the central molecule into the cluster, was compared with the sum of the formation energies of the dimers. If the dimer approximation is valid, their formation energy should add up to the total cohesion energy. Overall, the difference of the sum of all dimer interactions (-354.14 kJ mol^{-1}) and the computed cohesion energy approximation (-334 kJ mol^{-1}) is in the range of a few percent, confirming that the dimer approximation is a reasonable good approach to quantify and assess the interactions that govern the crystal structure stability.

An analysis analogous to the one carried out on Bi_2Naph_2 (**1**) was also performed for As_2Naph_2 (**2**), resulting in a 14-molecule cluster by taking all nearest neighbors of a central molecule in the unit cell. Fig. 6A depicts the 11 unique dimers that can be extracted from this structure, with two of these dimers ('Side X-like' and 'Front Upright') being twice inside the cluster while all others occur only once. Note that the 'Side X-like' dimer is similar to the 'Side X' dimers in the bismuth structure, in structure and interaction energy Fig. 6B depicts a comparison of the dimer formation energies and the cohesion energy of the cluster (-305.28 kJ mol^{-1}) in comparison with the dimer sum (-324.05 kJ mol^{-1}). Here, a slightly larger error (6.15%) than for Bi is observed. However, the per dimer error is still low enough (0.5%) to consider the dimer model a good approximation.

Comparing the analyses of the two structures reveals that the 'Top Y' is the one dominating the interaction in the structure of **1**, accounting for half of the total cohesion energy. In the case of **2**, the contributions are more evenly distributed

Open Access Article. Published on 01 March 2022. Downloaded on 2/14/2026 10:43:23 PM.
This article is licensed under a Creative Commons Attribution-NonCommercial 3.0 Unported Licence.

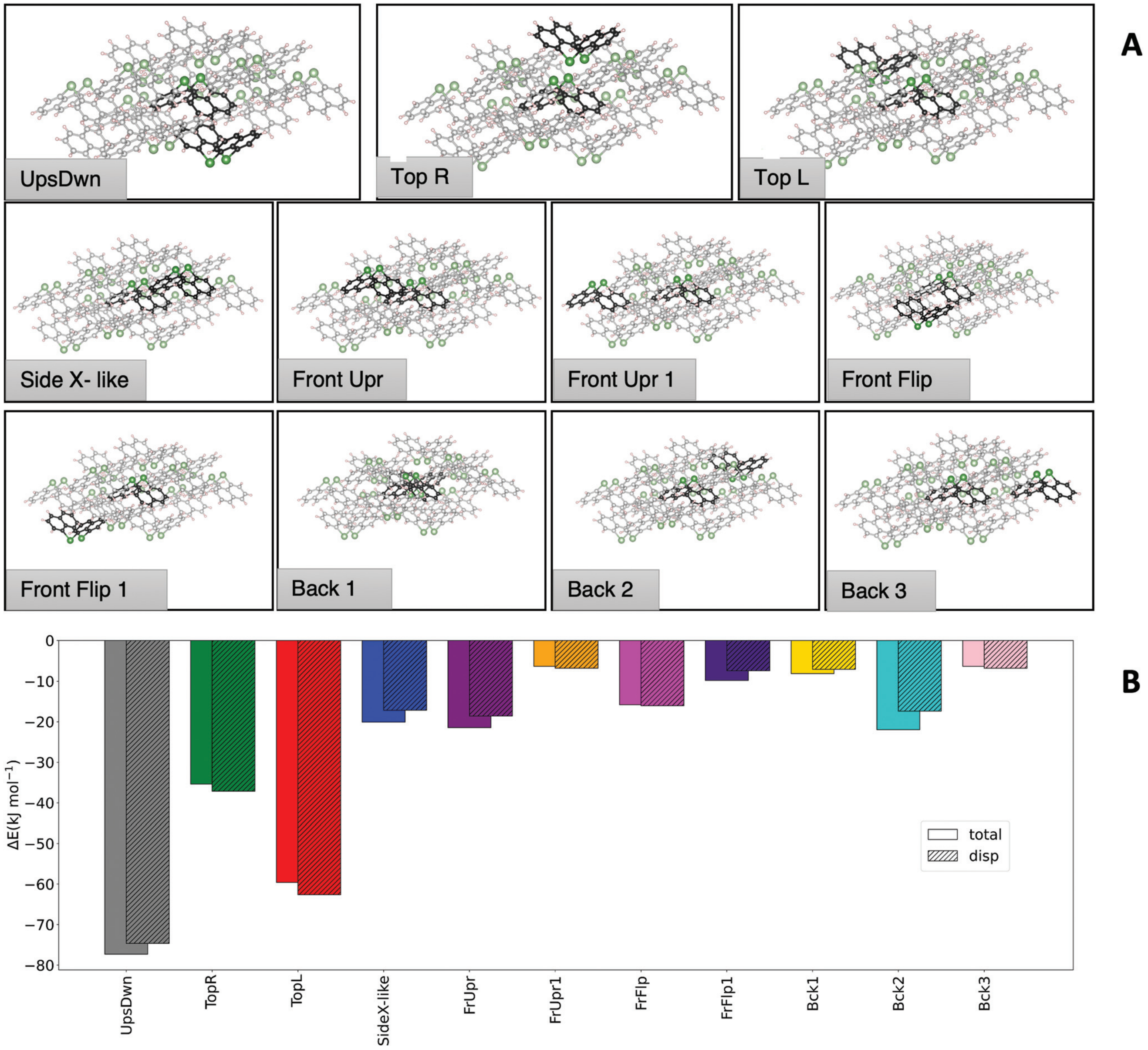

Fig. 6 (A) Dimers as cut from the 14-molecule cluster of As_2Naph_2 (**2**). Geometries are frozen at the experimental crystallographic ones. The highlighted molecules are the ones included in the calculations (see text) while the rest of the cluster is only shown to illustrate how the dimers were extracted. Colour code: C (black), As (green), H (light pink). (B) Comparison between the different dimer formation energies at the PBE0/def2-TZVPP level of theory.

across the dimers with two dominating dimer motifs. The largest contribution (*i.e.* 'UpsDwn') accounts for roughly 25% of the cohesion energy, followed by 'Top L' that contributes approximately 20% and 'Top R' and 'FrUpr' giving another ~13%. The remaining energy is distributed almost evenly among the other dimers. It should also be noted that the overall cohesion energy is lower for the As cluster, despite having one additional contact compared to Bi. Having established how the total cohesion energy of the different structures is dominated by certain dimer motifs, we now assess how the interaction energies for these specific dimers change for the pnictogens. For this purpose, we optimized the most significant dimers of both structures for the P, As, Sb and Bi compounds. This way, the dimers that occur in the Bi structure are computed also for As and *vice versa*.

Fig. 7B depicts the dimers and Fig. 7A the dimer formation energies for the different central atoms and the latter exhibits the reason for the preference of different pnictogens for different crystal structures: first of all, the 'Top Y' dimer is much more stable than the 'UpsDwn' dimer for Bi. Going from lighter elements to Bi, a switch from 'UpsDwn' to 'Top Y' stabilizes the structure by roughly 35 kJ mol^{-1}, if we account for the fact that the 'Top Y' dimer occurs twice. This brings us again to the conclusion that the Bi_2Naph_2 structure is driven

Open Access Article. Published on 01 March 2022. Downloaded on 2/14/2026 10:43:23 PM.
This article is licensed under a Creative Commons Attribution-NonCommercial 3.0 Unported Licence.

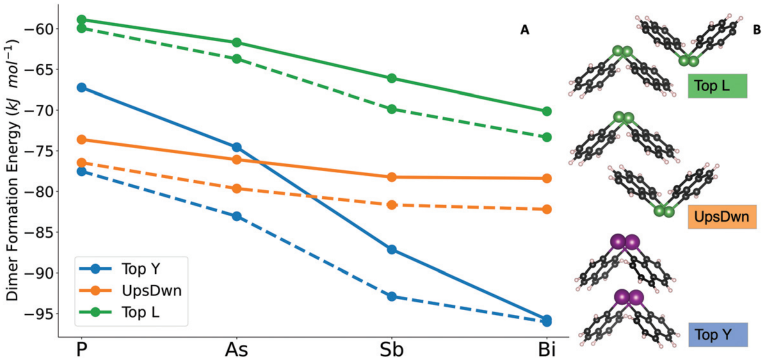

Fig. 7 (A) Total formation energies (solid lines) and dispersion contribution (dashed lines) of the dimers optimized at the PBE0/def2-TZVPP. (B) Dimers optimized at the PBE0/def2-TZVPP level of theory shown with the central atom from their original crystal structure. Optimizations have been performed also changing the central atom in each structure, going down the pnictogen group, from P to Bi. Colour code: Bi (purple), As (green), C (black), H (light pink).

by the formation of this very stable dimer, which in turn determines the aggregation of the others around it, whereas the difference is much less pronounced for As_2Naph_2 (**2**). However, we can still see that the 'UpsDwn' dimer, which occurs in the arsenic crystal structure, has a larger formation energy than 'Top Y'. As discussed above, for **2** the contributions to the cohesion energy are more homogeneously distributed between different dimers. While 'UpsDwn' is the strongest one, it is not the only driving force to the formation of this crystal structure, which is the result of different dimer contributions.

With increasing atomic number of the pnictogen atom, a steady increase in interaction energy is observed. Since the heavier atoms are better dispersion energy donors, the 'Top Y' dimer is the one that maximizes the dispersion dominated interactions between the central pnictogen and the aromatic rings.[32,33] Increased dispersion in the dimer interactions is in fact the main cause for the observed differences in the crystal structures. Electrostatics and covalent contributions, which are included in the "non-dispersive" part of the interaction (*i.e.* total interaction energy minus dispersion contribution)[29] do not play a major role in the dimer interactions. Note that an in-depth analysis of the nature of the interaction has been published previously.[33,34] Moving down the group, the 'Top Y' structure becomes more favorable with respect to the others, leading to a presumed crossover of the most stable crystal structure around Sb.

Conclusion

Pn_2Naph_2 (E = Bi **1**, As **2**) were synthesized and structurally characterized. Quantum chemical computations showed that energetic contribution from LDF play a key role in determining the crystal structures. The packing of dibismuthane **1** is driven by a single dimer interaction (Top Y), including Bi⋯π contacts, while in the case of diarsane **2** a more even distribution of interaction energies is found. By interchanging the Pn atoms within the most prominent dimers a clear trend was found, with Pn⋯π becoming increasingly stable with increasing atomic number, resulting in different structures within the Pn_2Naph_2 series.

Experimental

Materials and methods

General considerations. All manipulations were performed in an atmosphere of purified argon using standard Schlenk and glovebox techniques. Toluene, *n*-hexane and Et_2O were dried using an mBraun Solvent Purification System (SPS). CH_2Cl_2 and fluorobenzene were dried over CaH_2, while THF was carefully dried over NaK. Dried solvents were degassed and stored over appropriate molecular sieves. THF-d_8 and C_6D_6 were dried over activated molecular sieves (4 Å) and degassed prior to use. The anhydrous nature of the solvents was verified by Karl Fischer titration. Water was degassed through reflux in Ar atmosphere, followed by distillation. 1,8-Li_2Naph was prepared by a literature method.[35] 1,8-Br_2Naph and *n*-BuLi (2.5 M in *n*-hexane) were commercially available and used without further purification, whereas $AsCl_3$ and $BiCl_3$ were purified by distillation and sublimation prior to use. Microanalyses were performed at the Elemental Analysis Laboratory of the University of Duisburg-Essen. Melting points were measured using a Thermo Scientific 9300 apparatus. NMR spectra were recorded using a Bruker Avance Neo 400 (^1H = 400.1 MHz) or Bruker Avance III HD 600 (^1H: 600.1 MHz; $^{13}C\{^1H\}$: 150.9 MHz) spectrometer, and the spectra were referenced to internal C_6D_5H (^1H: δ = 7.16 ppm) or C_4D_7HO (^1H: δ = 1.72 ppm; ^{13}C: δ = 25.31 ppm). IR spectra were recorded with an ALPHA-T FT-IR spectrometer equipped with a single reflection ATR sampling module in a glovebox to guarantee measurements under inert gas conditions.

Synthetic procedures

Synthesis of Bi_2Naph_2 (1). Li_2Naph (6 mmol, 1.107 g) was weighed into a Schlenk tube and dissolved in 20 mL of thf. The green solution was cooled to −30 °C and a solution of

Open Access Article. Published on 01 March 2022. Downloaded on 2/14/2026 10:43:23 PM.
This article is licensed under a Creative Commons Attribution-NonCommercial 3.0 Unported Licence.

$BiCl_3$ (4 mmol, 1.241 g) in 50 mL of thf was added dropwise within two hours. The mixture was stirred for 12 h upon slowly warming to ambient temperature, yielding an orange suspension. Volatiles were removed *in vacuo*, 50 mL of degassed water was added and the suspension heated to 50 °C for 30 minutes, giving a yellow powder which was isolated by filtration and washed with hot *n*-hexane (4 × 25 mL). After the solvent was removed *in vacuo*, the product was extracted with hot toluene. The hot toluene solutions were filtered into a preheated Schlenk tube and allowed to cool in an oil bath, leading to the formation of yellow, crystalline needles, which were suitable for X-ray diffraction. Toluene was removed by filtration and the needles dried *in vacuo*.

Yield: 3%; m.p.: 320 °C (dec.); elemental analysis [wt%]: calcd for: $C_{20}H_{12}Bi_2$: C 35.8, H 1.80; found: C 34.2, H 1.56; ^{1}H NMR (600.1 MHz, 297 K, thf-d_8) δ [ppm]: 8.11 (dd, $^3J_{HH} = 6.59$ Hz, $^4J_{HH} = 1.09$ Hz, 2 H, Naph-2,7-C*H*), 7.35 (dd, $^3J_{HH} = 7.98$ Hz, $^4J_{HH} = 0.95$ Hz, 2 H, Naph-4,5-C*H*), 7.31 (dd, $^3J_{HH} = 7.84$, $^3J_{HH} = 6.75$ Hz, 2 H, Naph-3,6-C*H*); $^{13}C\{^1H\}$ NMR (150.9 MHz, 297 K, thf-d_8) δ [ppm]: 142.72 (Naph-2,7-*C*H), 127.80 (Naph-3,6-*C*H), 127.34 (Naph-4,5-*C*H); IR ν [cm^{-1}]: 3032 (w), 1529 (w), 1478 (w), 1424 (w), 1343 (w), 1187 (w), 1129 (w), 974 (w), 907 (w), 800 (s), 767 (s), 728 (w), 538 (w), 520 (w), 424 (m), 379 (w).

Synthesis of As_2Naph_2 (2). Li_2Naph (12 mmol, 2.245 g) was weighed into a Schlenk tube and dissolved in 20 mL of thf. The green solution was cooled to −40 °C and $AsCl_3$ (8 mmol, 1.45 g, 0.67 mL) dissolved in 50 mL of thf was added dropwise within two hours. The mixture was stirred for 12 h upon slowly warming to ambient temperature, yielding an orange suspension. Volatiles were removed *in vacuo*, 50 mL of degassed water was added and the resulting mixture was stirred for 30 minutes, giving a yellow powder which was isolated by filtration and washed with hot *n*-hexane (2 × 50 mL). After the solvent was removed *in vacuo*, the product was extracted with 100 mL of hot toluene. The toluene solution was stored at −30 °C to give yellow crystals of **2** which were isolated by filtration, washed with diethyl ether and dried *in vacuo*. Recrystallisation from fluorobenzene yielded the described polymorph of **2**. Analytical data match the previously reported ones.[2]

Yield: 300 mg (19%); ^{1}H NMR (400.1 MHz, 297 K, C_6D_6) δ [ppm]: 7.80 (dd, $^3J_{HH} = 6.94$ Hz, $^4J_{HH} = 0.89$ Hz, 2 H, Naph-2,7-C*H*), 7.24 (dd, $^3J_{HH} = 8.25$ Hz, $^4J_{HH} = 0.91$ Hz, 2 H, Naph-4,5-C*H*), 7.07 (dd, $^3J_{HH} = 8.12$, $^3J_{HH} = 6.96$ Hz, 2 H, Naph-3,6-C*H*).

Crystallography

The crystals were mounted on nylon loops in inert oil. Data were collected on a Bruker AXS D8 Kappa diffractometer with APEX2 detector ($Mo_{K\alpha}$ radiation, $\lambda = 0.71073$ Å) (**1**) and on a Bruker AXS D8 Venture diffractometer with a Photon II detector ($Cu_{K\alpha}$ radiation, $\lambda = 1.54178$ Å, microfocus source) (**2**) at 100(2) K. The structures were solved by Direct Methods (SHELXS-2013)[36] and refined anisotropically by full-matrix least-squares on F^2 (SHELXL-2017).[37,38] Absorption corrections were performed semi-empirically from equivalent reflections on the basis of multi-scans (**2**) and numerical from indexed faces (**1**) (Bruker AXS APEX3), respectively. Hydrogen atoms were refined using a riding model.

Conflicts of interest

There are no conflicts to declare.

Acknowledgements

Financial support by the Deutsche Forschungsgemeinschaft (S. S. SCHU 1069/19-2; A. A. A. AU 206/6-2) and the Max-Planck-Institut für Kohlenforschung (A. A. A. and E. S.) is acknowledged.

Notes and references

1 P. R. Schreiner, L. V. Chernish, P. A. Gunchenko, E. Y. Tikhonchuk, H. Hausmann, M. Serafin, S. Schlecht, J. E. P. Dahl, R. M. K. Carlson and A. A. Fokin, *Nature*, 2011, **477**, 308.

2 P. P. Power, *Organometallics*, 2020, **39**, 4127.

3 D. J. Liptrot and P. P. Power, *Nat. Rev. Chem.*, 2017, **1**, 0004.

4 P. Pyykkö, *Chem. Rev.*, 1997, **97**, 597.

5 J. Jung, S. T. Löffler, J. Langmann, F. W. Heinemann, E. Bill, G. Bistoni, W. Scherer, M. Atanasov, K. Meyer and F. Neese, *J. Am. Chem. Soc.*, 2020, **142**, 1864.

6 J. Oddershede and S. Larsen, *J. Phys. Chem. A*, 2004, **108**, 1057.

7 (*a*) P. Kilian, F. R. Knight and J. D. Woollins, *Chem. – Eur. J.*, 2011, **17**, 2302; (*b*) B. A. Chalmers, K. S. Athukorala Arachchige, J. K. D. Prentis, F. R. Knight, P. Kilian, A. M. Z. Slawin and J. D. Woollins, *Inorg. Chem.*, 2014, **53**, 8795.

8 (*a*) E. Hupf, E. Lork, S. Mebs, L. Chęcińska and J. Beckmann, *Organometallics*, 2014, **33**, 7247; (*b*) B. A. Chalmers, M. Bühl, K. S. Athukorala Arachchige, A. M. Z. Slawin and P. Kilian, *Chem. – Eur. J.*, 2015, **21**, 7520; (*c*) R. Arias Ugarte, D. Devarajan, R. M. Mushinski and T. W. Hudnall, *Dalton Trans.*, 2016, **45**, 11150; (*d*) B. A. Chalmers, C. B. E. Meigh, P. S. Nejman, M. Bühl, T. Lébl, J. D. Woollins, A. M. Z. Slawin and P. Kilian, *Inorg. Chem.*, 2016, **55**, 7117; (*e*) S. Furan, E. Hupf, J. Boidol, J. Brünig, E. Lork, S. Mebs and J. Beckmann, *Dalton Trans.*, 2019, **48**, 4504; (*f*) P. S. Nejman, T. E. Curzon, M. Bühl, D. McKay, J. D. Woollins, S. E. Ashbrook, D. B. Cordes, A. M. Z. Slawin and P. Kilian, *Inorg. Chem.*, 2020, **59**, 5616.

9 A. Gehlhaar, C. Wölper, F. van der Vight, G. Jansen and S. Schulz, *Eur. J. Inorg. Chem.*, DOI: 10.1002/ejic.202100883.

10 (*a*) T.-P. Lin, C. R. Wade, L. M. Pérez and F. P. Gabbaï, *Angew. Chem.*, 2010, **122**, 6501, (*Angew. Chem. Int. Ed.*, 2010, **49**, 6357); (*b*) C. R. Wade, T.-P. Lin, R. C. Nelson, E. A. Mader, J. T. Miller and F. P. Gabbaï, *J. Am. Chem. Soc.*, 2011, **133**, 8948.

This journal is © The Royal Society of Chemistry 2022

Open Access Article. Published on 01 March 2022. Downloaded on 2/14/2026 10:43:23 PM.
This article is licensed under a Creative Commons Attribution-NonCommercial 3.0 Unported Licence.

11 K. T. Mahmudov, A. V. Gurbanov, V. A. Aliyeva, G. Resnati and A. J. Pombeiro, *Coord. Chem. Rev.*, 2020, **418**, 213381.

12 (*a*) C. Ganesamoorthy, S. Heimann, S. Hölscher, R. Haack, C. Wölper, G. Jansen and S. Schulz, *Dalton Trans.*, 2017, **46**, 9227; (*b*) K. Dzialkowski, A. Gehlhaar, C. Wölper, A. A. Auer and S. Schulz, *Organometallics*, 2019, **38**, 2927.

13 M. Baba and T. Mizuta, *Polyhedron*, 2015, **92**, 30.

14 A.-M. Preda, M. Krasowska, L. Wrobel, P. Kitschke, P. C. Andrews, J. G. MacLellan, L. Mertens, M. Korb, T. Rüffer, H. Lang, A. A. Auer and M. Mehring, *Beilstein J. Org. Chem.*, 2018, **14**, 2125.

15 F. Neese, A. Hansen, F. Wennmohs and S. Grimme, *Acc. Chem. Res.*, 2009, **42**, 641.

16 F. Neese, A. Hansen and D. G. Liakos, *J. Chem. Phys.*, 2009, **131**, 064103.

17 C. Riplinger and F. Neese, *J. Chem. Phys.*, 2013, **138**, 034106.

18 C. Riplinger, P. Pinski, U. Becker, E. F. Valeev and F. Neese, *J. Chem. Phys.*, 2016, **144**, 024109.

19 D. G. Liakos, A. Hansen and F. Neese, *J. Chem. Theory Comput.*, 2011, **7**, 76.

20 P. J. Stephens, F. J. Devlin, C. F. Chabalowski and M. J. Frisch, *J. Phys. Chem.*, 1994, **98**, 11623.

21 J. P. Perdew, K. Burke and M. Ernzerhof, *Phys. Rev. Lett.*, 1996, **77**, 3865.

22 C. Adamo and V. Barone, *J. Chem. Phys.*, 1999, **110**, 6158.

23 J. Tao, J. P. Perdew, V. N. Staroverov and G. E. Scuseria, *Phys. Rev. Lett.*, 2003, **91**, 146401.

24 Y. Zhao and D. G. Truhlar, *Theor. Chem. Acc.*, 2008, **120**, 215.

25 A. D. Becke, *Phys. Rev. A*, 1988, **38**, 3098.

26 F. Weigend and R. Ahlrichs, *Phys. Chem. Chem. Phys.*, 2005, **7**, 3297.

27 S. Grimme, J. Antony, S. Ehrlich and H. Krieg, *J. Chem. Phys.*, 2010, **132**, 154104.

28 S. Grimme, S. Ehrlich and L. Goerigk, *J. Comput. Chem.*, 2011, **32**, 1456.

29 W. B. Schneider, G. Bistoni, M. Sparta, M. Saitow, C. Riplinger, A. A. Auer and F. Neese, *J. Chem. Theory Comput.*, 2016, **12**, 4778.

30 G. Bistoni, A. A. Auer and F. Neese, *Chem. – Eur. J.*, 2017, **23**, 865.

31 F. Neese, *Wiley Interdiscip. Rev.: Comput. Mol. Sci.*, 2018, **8**, e1327.

32 M. Krasowska, W. B. Schneider, M. Mehring and A. A. Auer, *Chem. – Eur. J.*, 2018, **24**, 10238.

33 M. Krasowska, A.-M. Fritzsche, M. Mehring and A. A. Auer, *ChemPhysChem*, 2019, **20**, 2539.

34 E. Schiavo, K. Bhattacharyya, M. Mehring and A. A. Auer, *Chem. – Eur. J.*, 2021, **27**, 14520.

35 R. L. Letsinger, J. A. Gilpin and W. J. Vullo, *J. Org. Chem.*, 1962, **27**, 672.

36 G. M. Sheldrick, *Acta Crystallogr., Sect. A: Found. Crystallogr.*, 1990, **A46**, 467.

37 G. M. Sheldrick, *Acta Crystallogr., Sect. C: Struct. Chem.*, 2015, **C71**, 3.

38 C. B. Hübschle, G. M. Sheldrick and B. Dittrich, shelXle, *A Qt GUI for SHELXL*, *J. Appl. Crystallogr.*, 2011, **44**, 1281.